

# P13.1 MULTIPLE-DOPPLER RADAR OBSERVATIONS OF VERTICAL WIND PROFILE HETEROGENEITY IN CONVECTIVE BOUNDARY LAYERS

PAUL MARKOWSKI\* AND YVETTE RICHARDSON

*Department of Meteorology, Pennsylvania State University, University Park, PA*

## 1. Introduction

The heterogeneity of the thermodynamic and kinematic state of the atmosphere has received increased appreciation in the last decade within the severe storms community, probably due in part to dense observations obtained from some recent field experiments as well as recent simulation studies demonstrating sensitivity of convective storms to small thermodynamic and wind shear perturbations. Weckwerth et al. (1996) showed that the thermodynamic variability observed among soundings within the boundary layer strongly depends on whether the sounding is launched through the updraft or downdraft of circulations induced by boundary layer convective overturning. Soundings launched through a boundary layer updraft depicted deeper, richer moist layers, implying less convective inhibition (CIN) and larger convective available potential energy (CAPE) than nearby soundings launched through a boundary layer downdraft, where lesser moisture concentrations and relatively shallow moist layers were indicated. Brooks et al. (1996) documented substantial thermodynamic heterogeneity revealed by soundings launched during the Verification of the Origins of Rotation in Tornadoes Experiment (VORTEX). Markowski et al. (1998) also documented heterogeneity revealed by VORTEX soundings, but in the storm-relative helicity (SRH) values derived from the sounding wind profiles. It cannot be known to what degree the variability documented by Brooks et al. and Markowski et al. was due to mesoscale processes versus boundary layer convection.

Work is currently underway to obtain a much more complete picture of the heterogeneity present in environments favorable for convective storms than can be gleaned from soundings alone. Our goal is to document the spatial and temporal variability of vertical wind profiles in convective boundary layers and to relate the variability to the organization of boundary layer convection. In this preprint, we present the research we have completed to date. What follows below are analyses derived from a ground-based mobile radar data set obtained during the International H<sub>2</sub>O Project (IHOP). An overview of these data and the wind synthesis methods is provided in the next section. Sections 3–5 contain examples of the time and space variability of hodographs and the vertical wind shear parameters derived from them. Some closing remarks are provided in section 6.

## 2. The 12 June 2002 IHOP case

Radar data from four truck-borne radars were obtained on 12 June 2002 in northwestern Oklahoma as part of an IHOP deployment designed to study convection initiation. The  $50 \times 50 \text{ km}^2$  analysis domain is approximately bisected in the west-east direction by an outflow boundary that was produced by thunderstorms occurring during the overnight hours (Fig. 1). A dryline is present in the eastern portion of the domain. Westward propagating gravity waves are observed in the outflow air mass. Boundary layer convection dominates the kinematic fields on both sides of the outflow boundary. There is some weak suggestion of organization into rolls and cells at some analysis times, especially on the warm side of the outflow boundary, although Weckwerth et al. (1997) probably would classify the convection as being disorganized on average. Maximum vertical velocity magnitudes at 1 km are approximately  $3 \text{ m s}^{-1}$  on the warm side of the outflow boundary and approximately  $2 \text{ m s}^{-1}$  on the cool side of the outflow boundary. Shallow cumulus clouds were observed within the data analysis region at the times showcased in the forthcoming sections, although some towering cumulus clouds developed along the outflow boundary at later times (2100–2130 UTC). Cumulonimbus clouds were initiated east of the analysis region along a dryline during the same time period.

The radar data used for the analyses were obtained from two Doppler On Wheels (DOW) radars (Wurman et al. 1997), the XPOL radar (specifications are similar to the DOWs), and the Shared Mobile Atmospheric Research and Teaching (SMART) radar (Biggerstaff and Guynes 2000). Radial velocity errors caused by low signal-to-noise ratio, second-trip echoes, sidelobes, ground clutter, and velocity aliasing were removed prior to interpolating the data to the  $50 \times 50 \text{ km}^2$  Cartesian grid. The grid has a horizontal and vertical grid spacing of 100 m. The domain is 2 km deep, which is approximately the depth of the boundary layer within which sufficient scatterers were present to allow for robust radial velocity measurements. Interpolation of the radial velocity data to the grid was accomplished with a Barnes objective analysis (Barnes 1964; Koch et al. 1983) using an isotropic, spherical weight function and smoothing parameter,  $\kappa$ , of  $0.36 \text{ km}^2$ . Advection was removed from the objectively analyzed radial velocity grids using Matejka's (2002) technique for determining the advection velocity. The three-dimensional wind field was synthesized using the overdetermined dual-Doppler approach (e.g., Kessinger et al. 1987) and the anelastic mass continuity equation (integrated upward), rather than a direct triple-

---

\*Corresponding author address: Dr. Paul Markowski, Department of Meteorology, Pennsylvania State University, 503 Walker Building, University Park, PA 16802; e-mail: pmarkowski@psu.edu.

or quadruple-Doppler solution. The time resolution of the analyses is 90 s.

### 3. Horizontal heterogeneity in vertical wind shear fields

Fields of mean vertical wind shear and SRH in the 0–2 km layer derived from the multi-Doppler wind syntheses are displayed in Fig. 1. It is perhaps not surprising that the patterns of the mean shear and SRH fields are highly correlated (linear correlation,  $r \sim 0.85$ ). What is more striking is the spatial complexity of these fields. Values of 0–2 km mean shear (0–2 km SRH) range from  $0.5\text{--}7.5 \times 10^{-3} \text{ s}^{-1}$  ( $-60\text{--}180 \text{ m}^2 \text{ s}^{-2}$ ). The mean shear and SRH fields are shown as examples owing to their popularity within the severe storms forecasting community. There are obviously dozens of other indices derived from the wind field that could have been displayed. We have every reason to believe that fields of other indices are equally heterogeneous.

Multiple scales of variability are apparent in the mean shear and SRH fields. In the easterly low-level flow north of the outflow boundary, shear and SRH are larger on average than on the south (warm) side of the outflow boundary, probably a result of baroclinic vorticity generation on the north side of the outflow boundary similar to that described by Markowski et al. (1998). In addition to this larger-scale variability, convective-scale (1–10 km) variability also is apparent and is due to the perturbations in the horizontal wind components associated with boundary layer thermals.

In the 12 June 2002 case, a case in which a prominent wind shift occurred along a mesoscale boundary, the contribution to the total heterogeneity of the mean shear and SRH fields owing to mesoscale processes exceeds the contribution from boundary layer thermals; i.e., the standard deviation of the mean shear and SRH values within a region confined to one side of the outflow boundary is smaller than the difference between the mean shear and SRH values that are spatially averaged north of the outflow boundary and south of the outflow boundary. This is not to say that we consider the heterogeneity owing to boundary layer thermals to be trivial. The range of mean shear (SRH) values observed on either side of the outflow boundary (not *across* the outflow boundary) spans  $5 \times 10^{-3} \text{ s}^{-1}$  ( $100 \text{ m}^2 \text{ s}^{-2}$ ).

### 4. Time evolution of hodographs

Assuming a nonzero mean wind, the spatial heterogeneity documented in section 3 implies large temporal variability in the characteristics of vertical wind profiles at fixed locations. Hodographs are displayed at 3-min intervals over a 9-min period at four locations in the analysis domain (indicated by stars in Fig. 1) in Fig. 2. At some locations (e.g., top panels of Fig. 2), what we regard as fairly significant evolution is observed in the hodographs. Although the 0–2 km mean wind changes little during the 9-min period, the orientation of the 0–2 km shear vector (the ray drawn from the start to the end of the hodograph traces in Fig. 2) changed by as much as  $70^\circ$  during

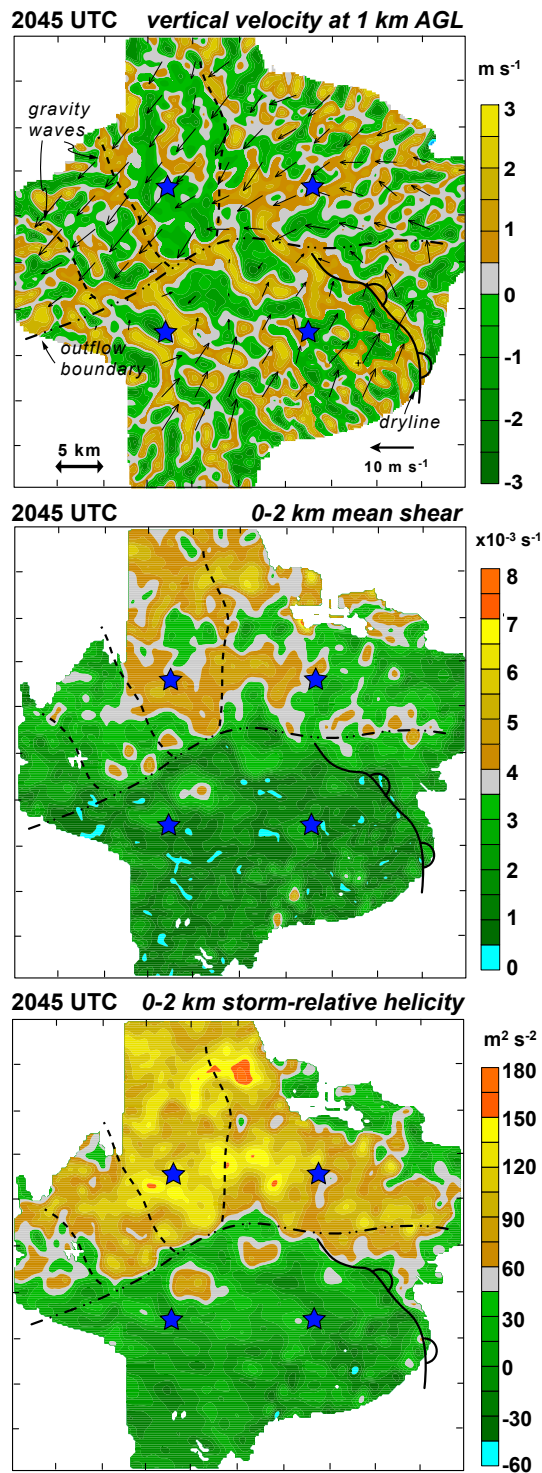


FIG. 1. Horizontal cross sections at 2045 UTC 12 June 2002 of (top) vertical velocity at 1.0 km and horizontal wind vectors at 0.1 km (the tail of each vector is located at every 20th grid point), (middle) mean vertical wind shear in the 0–2 km layer, and (bottom) storm-relative helicity (SRH) in the 0–2 km layer. The domain is  $50 \times 50 \text{ km}^2$  and is located in northwestern Oklahoma. The dash-dot line indicates an outflow boundary, the line with unfilled scallops indicates a dryline, and the dashed lines indicate gravity wave fronts. The four stars, located at  $x = \pm 8 \text{ km}$  and  $y = \pm 8 \text{ km}$  [the center of the domain is at (0,0)], indicate the locations from where the hodographs displayed in Figs. 2 and 3 were obtained.

this short time interval. Significant hodograph curvature changes also were possible, as were changes in hodograph length of up to a few  $\text{m s}^{-1}$  over the lowest 2 km.

## 5. Comments on “proximity soundings”

Since shortly after computing advancements allowed for the three-dimensional simulation of thunderstorms, so-called “proximity soundings” have been used to initialize numerical models in which the base state is horizontally homogeneous. Proximity soundings are intended to be representative of the ambient environment of the storm and have been obtained from either a single, fortuitous rawinsonde or by compositing several individual soundings launched at various ranges from a storm. Probably the most heavily used proximity sounding used in numerical simulation studies represents the environment of the Del City, Oklahoma, supercell on 20 May 1977 (Klemp et al. 1981; Klemp and Rotunno 1983; Grasso and Cotton 1995; Adlerman et al. 1999; Adlerman and Droegemeier 2002).

Many arguments have been made for the use of such proximity soundings. These arguments have included (1) the need to focus on the fundamental storm dynamics, which can most easily be accomplished if environmental heterogeneities are excluded; (2) lack of sufficiently detailed observations characterizing the heterogeneity; (3) difficulties in introducing heterogeneities owing to model imbalances that may result. We believe that the preceding justifications quite often have been valid, although we also echo the concerns expressed by Brooks et al. (1994, 1996). As model resolution becomes finer and finer and high-resolution “case study” or tornadogenesis simulations become favored over large parameter space studies, it may be more crucial to account for the complex interactions between storms and environmental heterogeneities. Indeed, Richardson (1999) showed significant changes in storm structure due to movement through environments characterized by spatially-varying vertical wind shear or moisture. Storm properties routinely exhibited a complex dependency on their history. In some cases, storm existence might not even be predicted based on only a sounding near the storm at that particular time.

The spatial and temporal variability of vertical wind profiles documented in sections 3 and 4 leads one to naturally wonder about the representativeness of proximity soundings derived from a single sounding or even from compositing several soundings. What is perhaps most disturbing is that considerable heterogeneity is present even *away from* the obvious mesoscale boundaries that may be detectable by today’s observing systems; i.e., much heterogeneity is present in regions that many investigators might have classified as “horizontally homogeneous” in the past.

It is also problematic that the heterogeneity implies that a hodograph obtained from a rawinsonde launched at a given location is likely to deviate from the true hodograph, as soundings rarely provide either instantaneous or truly vertical wind profiles. We have attempted to document the hodograph errors due to sounding drift through a heterogeneous atmosphere by constructing “pseudo-

hodographs,” which simulate the hodograph that would be traced by a rawinsonde. Each pseudohodograph was created by computing the trajectory that a balloon would take through the boundary layer. The horizontal wind components at each level were obtained by measuring the displacement of the hypothetical balloon in a 6-s time period, which approximately emulates the frequency at which navigational data are recorded by rawinsondes. A balloon ascent rate of  $5 \text{ m s}^{-1}$  was assumed. Each pseudohodograph calculation typically required 5–6 three-dimensional wind syntheses spanning 400–500 s given the assumed balloon ascent rate. As was the case for the true hodographs, the pseudohodographs only span the lowest 2 km.

Pseudohodographs (Fig. 3) were compared to the true hodographs at the same four locations at which the temporal hodograph changes were documented in Fig. 2. Differences in 0–2 km hodograph length of  $2 \text{ m s}^{-1}$  were noted between the pseudohodographs and true hodographs, which correspond to mean shear differences of  $0.001 \text{ s}^{-1}$ . These differences might not be what many would regard as large; however, differences in hodograph curvature and overall shape often were much more pronounced in comparing pseudohodographs to true hodographs (e.g., top left panel of Fig. 3). The differences between the pseudohodographs and true hodographs, in addition to the real, ubiquitous heterogeneity documented in sections 3 and 4, illustrate a potential difficulty in directly comparing observed storm behaviors and the (observed) pseudosoundings obtained from the storm environments to storm behaviors predicted by simulation or theoretical studies based on true soundings.

## 6. Future work

Our near-term plans include analyses of several additional cases that differ from the one showcased herein. We anticipate that it will be interesting to investigate some cases in which obvious mesoscale contributions to the heterogeneity are absent, i.e., cases in which the heterogeneity is entirely due to boundary layer convection structures. We also will examine the relationship between wind shear heterogeneity and additional boundary layer convection organizational modes, e.g., horizontal convective rolls and cellular convection. Additional ongoing research (e.g., Kost and Richardson 2004, Kron and Richardson 2004) uses three-dimensional simulations to examine storm sensitivity to mesoscale moisture and wind shear variability.

Farther down the road we plan to investigate how storms modify the boundary layer and any heterogeneity induced by boundary layer convection (e.g., beneath the leading anvil and precipitation regions). Ultimately we hope to develop a better understanding of how convective-scale variability impacts storms. Given the computing capabilities of today, we believe that it would be highly worthwhile to begin simulating storms with the inclusion of sensible heat fluxes and convective boundary layers (e.g., Carpenter et al. 1998), at least in high-resolution, “case study” or tornadogenesis simulations.

2036-2045 UTC

Hodographs

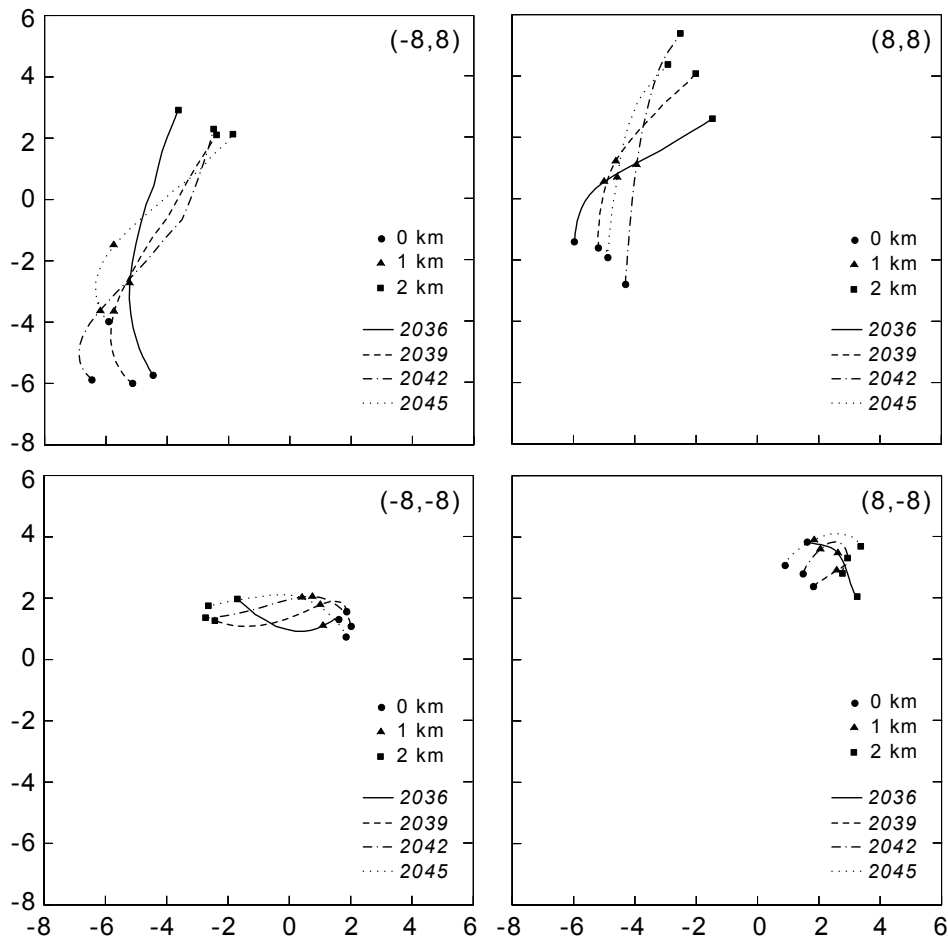


FIG. 2. Hodographs at 2036, 2039, 2042, and 2045 UTC 12 June 2002 obtained from the locations of the four stars indicated in Fig. 1 (the coordinates of the hodographs are displayed at the top right of each panel). Units on the axes are  $\text{m s}^{-1}$ . The 0, 1, and 2 km locations on the hodograph traces are indicated with filled circles, triangles, and squares, respectively.

#### REFERENCES

- Adlerman, E. J., and K. K. Droegemeier, 2002: The sensitivity of numerically simulated cyclic mesocyclogenesis to variations in model physical and computational parameters. *Mon. Wea. Rev.*, **130**, 2671–2691.
- Adlerman, E. J., K. K. Droegemeier, and R. Davies-Jones, 1999: A numerical simulation of cyclic mesocyclogenesis. *J. Atmos. Sci.*, **56**, 2045–2069.
- Barnes, S. L., 1964: A technique for maximizing details in numerical weather map analysis. *J. Appl. Meteor.*, **3**, 396–409.
- Biggerstaff, M. I., and J. Guynes, 2000: A new tool for atmospheric research. Preprints, *20th Conf. on Severe Local Storms*. Orlando, Amer. Meteor. Soc., 277–280.
- Brooks, H. E., C. A. Doswell, and J. Cooper, 1994: On the environments of tornadic and nontornadic mesocyclones. *Wea. Forecasting*, **9**, 606–618.
- Brooks, H. E., M. T. Carr, and J. E. Ruthford, 1996: Preliminary analysis of soundings from VORTEX-95. Preprints, *18th Conf. on Severe Local Storms*. San Francisco, Amer. Meteor. Soc., 133–136.
- Carpenter, R. L., K. K. Droegemeier, and A. M. Blyth, 1998: Entrainment and detrainment in numerically simulated cumulus congestus clouds. Part I: General results. *J. Atmos. Sci.*, **55**, 3417–3432.
- Grasso, L. D., and W. R. Cotton, 1995: Numerical simulation of a tornado vortex. *J. Atmos. Sci.*, **52**, 1192–1203.
- Kessinger, C. J., P. S. Ray, and C. E. Hane, 1987: The Oklahoma squall line of 19 May 1977. Part I: A multiple Doppler analysis of convective and stratiform structure. *J. Atmos. Sci.*, **44**, 2840–2864.
- Klemp, J. B., and R. Rotunno, 1983: A study of the tornadic region within a supercell thunderstorm. *J. Atmos. Sci.*, **40**, 359–377.
- Klemp, J. B., R. B. Wilhelmson, and P. S. Ray, 1981: Observed and numerically simulated structure of a mature supercell thunderstorm. *J. Atmos. Sci.*, **38**, 1558–1580.
- Koch, S. E., M. DesJardins, and P. J. Kocin, 1983: An interactive Barnes objective map analysis scheme for use with satellite and conventional data. *J. Clim. Appl. Meteor.*, **22**, 1487–1503.
- Kost, J., and Y. Richardson, 2004: The influence of temporally-varying vertical wind shear on numerically simulated convective storms. Preprints, *22nd Conf. on Severe Local Storms*. Hyannis, Massachusetts, Amer. Meteor. Soc.
- Kron, J., and Y. Richardson, 2004: The influence of horizontally-varying CAPE and vertical shear on numerically-simulated convective storms. Preprints, *22nd Conf. on Severe Local Storms*. Hyannis, Massachusetts, Amer. Meteor. Soc.
- Markowski, P. M., J. M. Straka, E. N. Rasmussen, and D. O. Blanchard, 1998: Variability of storm-relative helicity during VORTEX. *Mon. Wea. Rev.*, **126**, 2959–2971.
- Matejka, T., 2002: Estimating the most steady frame of reference from Doppler radar data. *J. Atmos. Oceanic Technol.*, **19**, 1035–1048.
- Richardson, Y. P., 1999: The influence of horizontal variations in vertical shear and low-level moisture on numerically simulated convective storms. Ph.D. Dissertation, Department of Meteorology, University of Oklahoma-Norman, 236 pp.
- Weckwerth, T. M., J. W. Wilson, and R. M. Wakimoto, 1996: Thermodynamic variability within the convective boundary layer due to horizontal convective rolls. *Mon. Wea. Rev.*, **124**, 769–784.
- Weckwerth, T. M., J. W. Wilson, R. M. Wakimoto, and N. A. Crook, 1997: Horizontal convective rolls: Determining the environmental conditions supporting their existence and characteristics. *Mon. Wea. Rev.*, **125**, 505–526.
- Wurman, J., J. Straka, E. Rasmussen, M. Randall, and A. Zahrai, 1997: Design and deployment of a portable, pencil-beam, pulsed, 3-cm Doppler radar. *J. Atmos. Oceanic Technol.*, **14**, 1502–1512.

2045 UTC

**Hodographs and Pseudohodographs**

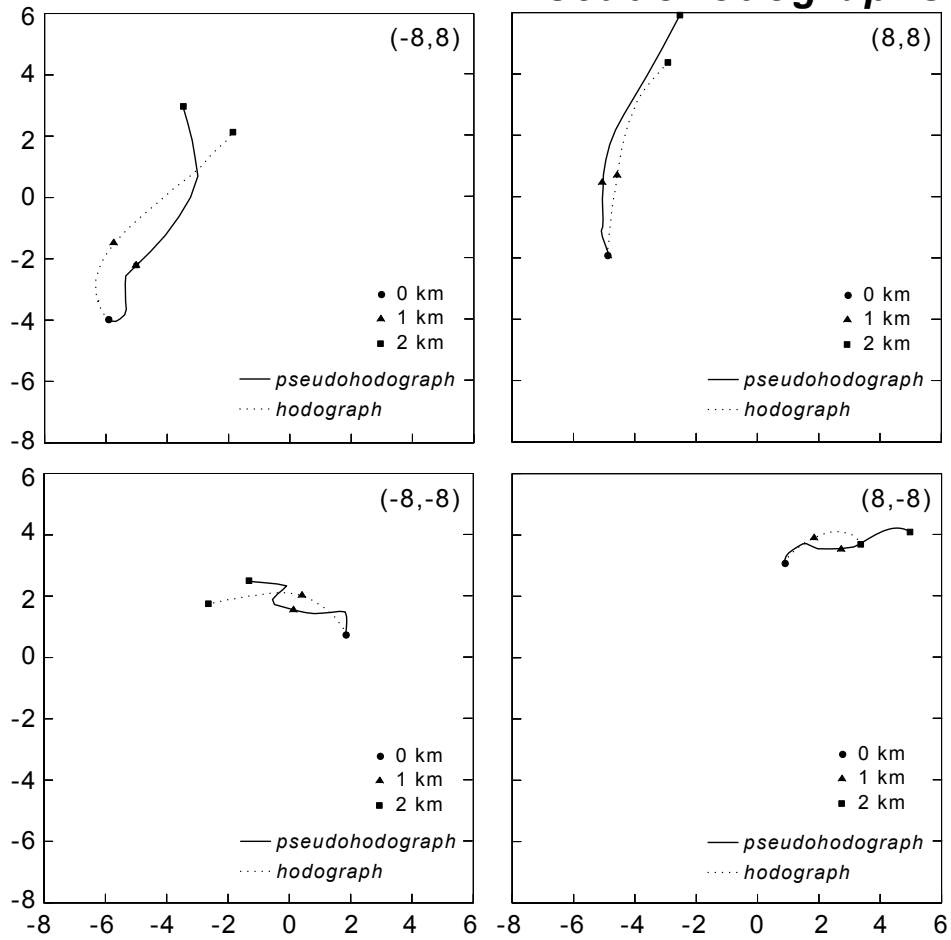


FIG. 3. Hodographs and pseudohodographs at 2045 UTC 12 June 2002 obtained from the locations of the four stars indicated in Fig. 1 (the coordinates of the hodographs are displayed at the top right of each panel). The pseudohodographs were obtained by assuming a balloon ascent rate of  $5 \text{ m s}^{-1}$ . Units on the axes are  $\text{m s}^{-1}$ . The 0, 1, and 2 km locations on the hodograph traces are indicated with filled circles, triangles, and squares, respectively.